Received: 16 February 2018 | Accepted: 26 April 2018

DOI: 10.1002/hyp.13150

RESEARCH ARTICLE

WILEY

Evaluating the functionality and streamflow impacts of explicitly modelling forest–snow interactions and canopy gaps in a distributed hydrologic model

Ning Sun[1] | Mark Wigmosta[1,3] | Tian Zhou[2] | Jessica Lundquist[3] | Susan Dickerson-Lange[4] | Nicoleta Cristea[3]

[1] Hydrology Technical Group, Pacific Northwest National Laboratory, Richland, WA 99352, USA

[2] Atmospheric Sciences & Global Change, Pacific Northwest National Laboratory, Richland, WA 99352, USA

[3] Department of Civil and Environmental Engineering, University of Washington, Seattle, WA 98195, USA

[4] Natural Systems Design, Seattle, WA 98195, USA

Correspondence
Ning Sun, Hydrology Technical Group, Pacific Northwest National Laboratory, Richland, WA 99352, USA.
Email: ning.sun@pnnl.gov

Funding information
U.S. Department of Defense Strategic Environmental Research and Development Program, Grant/Award Number: Project RC-2546

Abstract

Many plot-scale studies have shown that snow-cover dynamics in forest gaps are distinctly different from those in open and continuously forested areas, and forest gaps have the potential to alter the magnitude and timing of snowmelt. However, the watershed-level impacts of canopy gap treatment on streamflows are largely unknown. Here, we present the first research that explicitly assesses the impact of canopy gaps on seasonal streamflows and particularly late-season low flows at the watershed scale. To explicitly model forest–snow interactions in canopy gaps, we made major enhancements to a widely used distributed hydrologic model, distributed hydrology soil vegetation model, with a canopy gap component that represents physical processes of snowpack evolution in the forest gap separately from the surrounding forest on the subgrid scale (within a grid typically 10–150 m). The model predicted snow water equivalent using the enhanced distributed hydrology soil vegetation model showed good agreement ($R^2 > 0.9$) with subhourly snow water equivalent measurements collected from open, forested, and canopy gap sites in Idaho, USA. Compared with the original model that does not account for interactions between gaps and surrounding forest, the enhanced model predicted notably later melt in small- to medium-size canopy gaps (the ratio of gap radius (r) to canopy height (h) $\leq$ 1.2), and snow melt rates exhibited great sensitivity to changing gap size in medium-size gaps ($0.5 \leq r/h \leq 1.2$). We demonstrated the watershed-scale implications of canopy gaps on streamflow in the snow-dominated Chiwawa watershed, WA, USA. With 24% of the watershed drainage area (about 446 km^2) converted to gaps of 60 m diameter, the mean annual 7-day low flow was increased by 19.4% (i.e., 0.37 m^3/s), and the mean monthly 7-day low flows were increased by 13.5% (i.e., 0.26 m^3/s) to 40% (i.e., 1.76 m^3/s) from late summer through fall. Lastly, in practical implementation of canopy gaps with the same total gap areas, a greater number of distributed small gaps can have greater potential for longer snow retention than a smaller number of large gaps.

KEYWORDS

canopy gap, DHSVM, forest management, forest–snow interactions, snow hydrology, summer low flow

1 | INTRODUCTION

Snowmelt provides a critical source of runoff in the mountainous areas of mid- to high-latitudes (Barnett et al., 2008; Yan et al., 2018) and sustains summer low flow vital for healthy aquatic habitat. There has been growing recognition over the last century that snow accumulation and ablation in mountain forest environments depend critically on forest structure (Broxton et al., 2015; Connaughton, 1935; Moore & McCaughey, 1997; Pomeroy, Parviainen, Hedstrom, & Gray, 1998; Varhola, Coops, Weiler, & Moore, 2010). Despite climate and topographic impacts of varying degrees, many studies found that forested areas, in contrast to open areas, commonly accumulate less snow and thus produce less water available for runoff, due mainly to canopy interception and evapotranspiration of up to 60% of accumulated snow (Cristea, Lundquist, Loheide, Lowry, & Moore, 2014; Hedstrom & Pomeroy, 1998; Marks, Kimball, Tingey, & Link, 1998; McCabe & Clark, 2005; McCabe, Hay, & Clark, 2007; Pomeroy et al., 1998; Regonda, Rajagopalan, Clark, & Pitlick, 2005; Stednick, 1996; Stewart, Cayan, & Dettinger, 2005; Troendle & King, 1985). Prior studies generally agree that sparser forest canopy advances melt due to reduced radiation attenuation (Link & Marks, 1999; Troendle & King, 1985; Varhola et al., 2010). However, the opposite may occur when the enhanced longwave radiation under canopies offsets the reduction in shortwave radiation from canopy attenuation, a situation referred to as the "radiative paradox" (Ambach, 1974; Lundquist, Dickerson-Lange, Lutz, & Cristea, 2013; Reifsnyder & Lull, 1965; Seyednasrollah, Kumar, & Link, 2013; Sicart et al., 2004).

Snow surveys by Church (1933, 1912) in the early 1900s at various locations in the Sierra Nevada suggested the relationship between forest gaps and snow properties. Studies of the potential of forest gaps to promote snow accumulation and melt were later conducted by Kittredge (1953) and Anderson (1963) in the Sierra Nevada snow zone (above 1,500 m elevation). More recently, there has been a growing interest in opening gaps in the canopy as a forest management alternative to achieve a wide breadth of hydrological and ecological objectives at the watershed or greater scales typically ranging from 10 up to 10,000 km^2 (Kern et al., 2017; Lindner, Lasch, & Erhard, 2000; Nowak et al., 2013). With no snow interception, reduced downward longwave radiation, and the shelter effect of wind and solar radiation (i.e., shading) provided by the surrounding forest, many field observations indicated that small-size forest gaps have the potential to increase snow water storage and enhance snow retention (Berry & Rothwell, 1992; Dickerson-Lange et al., 2015; Golding & Swanson, 1986; Murray & Buttle, 2003; Varhola et al., 2010). In the Cedar River Watershed located on the western slope of the Cascade Range (characterized by a maritime climate) in the Pacific Northwest, the mean snow duration in a circular gap cut in the forest with a diameter of 20 m (equal to approximately one tree height) was observed to be 1–2 weeks longer than in the adjacent control forest covered by untreated second-growth forest dominated by western hemlock and Douglas-fir (Dickerson-Lange et al., 2015). These unique benefits of forest gaps have led to recent modelling developments that address the distinct radiation scheme in a forest gap from entirely open or forested areas (Lawler & Link, 2011; Musselman, Molotch, Margulis, Lehning, & Gustafsson, 2012), the energy budget at the forest gap floor (Seyednasrollah & Kumar, 2014), net canopy interception (Moeser, Morsdorf, & Jonas, 2015; Moeser, Stähli, & Jonas, 2015), and snow distributions (Broxton et al., 2015) in the presence of forest gaps.

Although these studies greatly advanced our knowledge of forest gaps, the implications for snow dynamics and streamflows in particular are largely unknown at the watershed and larger scales. Ellis, Pomeroy, and Link (2013) coupled a gap radiation model with the Cold Regions Hydrological Model (Fang et al., 2013; Pomeroy et al., 2007) to demonstrate the potential of forest gaps to alter snowmelt response, focusing especially on cold regions over spatially lumped hydrologic response units. In application to a Saskatchewan River headwater basin of the Canadian Rocky Mountains, Ellis et al. (2013) found that small forest gaps substantially increased the magnitude of spring snowmelt due to reductions in snow interception losses, whereas slope orientation showed a great impact on the timing of snowmelt, with accelerated snowmelt on south-facing slopes and delayed snowmelt on north-facing slopes. We use a more detailed approach than Ellis et al. (2013) to account for spatiotemporal pattern of radiation in gaps. More importantly, this is the first study that explicitly assesses the effects of canopy gaps on streamflows at the watershed scale.

Our model development features subgrid representation of forest–snow dynamics in canopy gaps. The development was made within the framework of an existing spatially distributed, physics-based hydrological model—the distributed hydrology soil vegetation model (DHSVM; Wigmosta, Vail, & Lettenmaier, 1994). DHSVM has been extensively applied for hydrologic modelling, particularly in complex mountainous environment typically at the 10–150 m spatial resolution and subhourly to daily time step (Bowling & Lettenmaier, 2001; Cao, Sun, Yearsley, Nijssen, & Lettenmaier, 2016; Cristea et al., 2014; Du, Link, Gravelle, & Hubbart, 2014; Jost, Moore, Weiler, Gluns, & Alila, 2009; Leung & Wigmosta, 1999; Livneh et al., 2015; Thyer, Beckers, Spittlehouse, Alila, & Winkler, 2004; Whitaker, Alila, Beckers, & Toews, 2002). In an extensive review of 30 hydrological models (Beckers, Smerdon, & Wilson, 2009), DHSVM was identified to be best suited for hydrologic modelling in forested environments over complex mountainous terrain because of its detailed process representation of topographic and canopy control of the energy and mass exchange in a spatially distributed manner. However, DHSVM's original model structure and radiation scheme are not suited for simulating forest cover that has gap openings. The original model partitions a forested grid into canopy-covered and open areas without accounting for interactions between the two (e.g., the surrounding forest does not shade the open areas), and treats the whole grid cell as a uniform, single snowpack (Figure 1). In the enhanced DHSVM, any model grid prescribed to have a canopy gap structure is partitioned into gap and surrounding forest, which are treated as independent snowpack governed by separate mass and energy input (Figure 1). The enhancement accounts explicitly for the impact of the surrounding forest (e.g., shading and wind attenuation) on the gap energy balance, and produces spatially varied irradiance with an idealized cylindrical gap geometry. Finally, the DHSVM architecture provides a highly scalable tool (from the plot to regional scale) that allows for snow hydrologic impact analysis of prescribed spatially explicit forest management strategies (e.g., forest gapping, thinning, and restoration) with process presentation of site-specific and

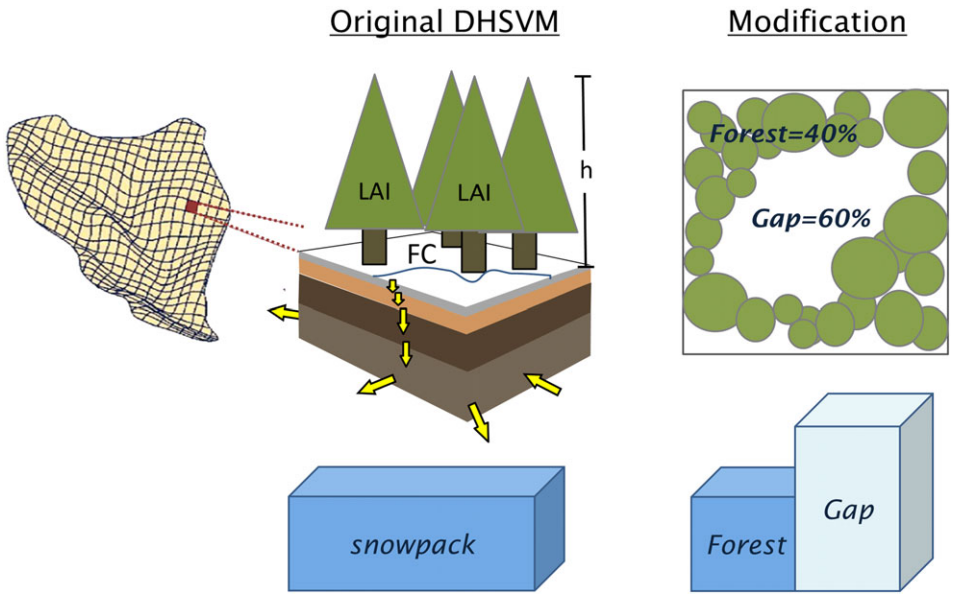

FIGURE 1 Grid representation of the canopy gap in the original and modified distributed hydrology soil vegetation model (DHSVM). In the DHSVM, forest canopy is characterized by leaf area index (*LAI*), canopy height (*h*), and fractional coverage (FC)

In this paper, we first present the new model development focusing on snowpack energy budget at the forest gap floor. We validate the enhanced model against measurements taken at three experimental sites that have distinct canopy covers and analyse the snow ablation dynamics in association with snow-cover energetics. We then evaluate the enhanced model structure (subgrid canopy classification) relative to the original structure (uniform grid) for snow modelling. Lastly, we present a simple watershed-scale application using the enhanced model to demonstrate the impact of gap implementation on streamflow seasonality; of particular interest are the summer low flows that are critical for socioecological systems such as salmon conservation.

2 | METHODS

2.1 | Overview of DHSVM and model enhancement

The DHSVM simulates snow processes on the grid scale with a two-layer canopy model and a two-layer below-canopy energy and mass balance snow model. The canopy snow model explicitly represents the combined canopy processes that govern snow interception, sublimation, mass release, and melt (Wigmosta et al., 1994; Wigmosta, Nijssen, Storck, & Lettenmaier, 2002). Spatial input files are used to assign each model grid a vegetation type (including canopy height), and, where appropriate, a gap diameter. An independent one-dimensional (vertical) coupled energy and water balance is calculated for each grid cell. The snowpack energy balance described in Equation (1) determines the net energy input to snowpack (ΔQ):

$$\Delta Q = \mathrm{NSW} + \mathrm{NLW} + \mathrm{H} + \mathrm{LE} + \mathrm{M} \quad (1)$$

where *NSW* is net shortwave radiation, *NLW* is net longwave radiation, *H* is sensible heat flux, *LE* is latent heat flux from evaporation and sublimation/condensation, and *M* is advected heat from rainfall to snowpack. All terms are in the unit of W/m^2. Conductive heat at the snow–ground interface is neglected. Flow is routed vertically based on a one-dimensional multilayer soil model, and laterally based on a quasi-three-dimensional saturated subsurface flow model. The core DHSVM model physics and structure in the original version are described in detail by Wigmosta et al. (1994), Storck, Bowling, Wetherbee, and Lettenmaier (1998), and Wigmosta et al. (2002).

The structure and radiation scheme in the original model are not suited for simulating forest cover with gap openings. In the original version, the model conceptualizes a grid cell as being composed of independent canopy-covered and open areas (Figure 1). The forested areas are lumped under a fractional coverage (FC) parameter and all gaps/open areas are represented by 1-FC. The forested areas under FC are assumed to be continuous, and any small openings in the canopy are implicitly accounted for in the leaf area index (*LAI*) term. Separate, independent energy-balance calculations are performed at each time step for the open fraction and the forested fraction, and no interaction occurs between the two fractions (e.g., the surrounding forest does not shade the open areas). The grid-average mass and energy input from the two fractions are then used to calculate snowmelt for the grid cell, which is treated as a uniform, single snowpack. With enhancement, any model grid prescribed with a canopy gap structure (i.e., gap diameter > 0) is partitioned into gap and surrounding forest components, each with a separate snowpack governed by its own mass and energy input (Figure 1). The enhanced model accounts explicitly for the impact of surrounding forest (e.g., shading and wind attenuation) on the gap energy balance. We built our grid-scale canopy gap radiative scheme based on the center-point radiation model described by Ellis et al. (2013), which extended the point-scale radiation scheme by Lawler and Link (2011) to estimate the mean shortwave radiation in a forest gap using the shortwave radiation to the centre of the gap base. This center-point approach, as evaluated by Ellis et al. (2013), considerably overestimates the mean gap radiation during the melt period when sol

this issue, our approach explicitly accounts for the circular gap geometry when calculating the light attenuation path to the gap base and hence spatially distributed irradiance. The model assumes no snow interception in canopy gaps, and the surrounding forest portion intercepts snow the same as continuous forest.

2.2 | Gap-adjusted irradiance

We describe our grid-scale radiative scheme for the gap snowpack (i.e., the gap portion of a grid) and provide formulations below. We adopted the commonly used cylindrical shape to characterize a forest gap, as in Lawler and Link (2011) and Ellis et al. (2013; Figure 2). This cylindrical setup simplifies the radiation calculations because the cylindrical (gap) surface can be positioned to remain normal to the sun's beam as the surface-solar azimuth angle changes. The surrounding forest is treated as continuous forest canopy, and its radiation fluxes are calculated using the original DHSVM formulations. It is assumed that shortwave radiation (including both direct and diffuse radiation) in the surrounding forest is not influenced by adjacent gaps. Observations have demonstrated that ablation rates within the adjacent forest differ based on position relative to the gap, due to the influence of direct solar radiation passing between trees as well as the solar heating of tree stems (Lawler & Link, 2011; Pomeroy et al., 2009). Thus, this assumption represents a simplification that could be addressed in future work.

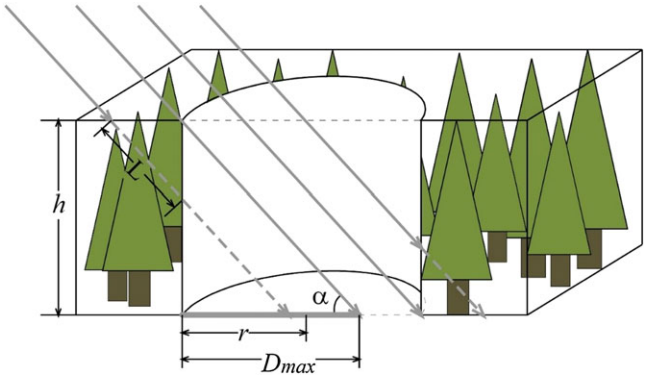

FIGURE 2 Schematic of a cylindrical forest gap with canopy height *h* and radius *r*, where *L* is attenuation path length, *α* is solar altitude of incoming light, and D_{max} is maximum shadow length. Direct radiation is represented by solid lines, and attenuated radiation is represented by dotted lines

2.2.1 | Beam shortwave radiation

The original radiation regime in the DHSVM estimates light attenuation through the canopy as a function of *LAI* and a fixed canopy attenuation coefficient (λ) that does not change with time or solar elevation (Equation (2)). For more accurate estimation of radiative input, we used the Beer-Bouger-Lambert law (Peixoto & Oort, 1992) to estimate radiation transmission (Equation (3)), which explicitly considers the interactions between canopy and solar geometry in estimation of radiation transmission through canopy. The algorithm is based on that of Link and Marks (1999), with the exception that the model now allows the extinction coefficient (*k*) to vary monthly.

$$\tau_b = e^{-\lambda \cdot LAI} \tag{2}$$

$$\tau_b = e^{-k \cdot L} = e^{-k \cdot \frac{h}{\sin\alpha}} \tag{3}$$

where τ_b is the fraction of shortwave radiation transmitted through the canopy, *L* is light attenuation length through the canopy calculated as a function of canopy height (*h*) and solar elevation (*α*), and *k* is the *LAI*-dependent radiation extinction coefficient, which varies monthly (Sun, Yearsley, Voisin, & Lettenmaier, 2015).

Within a canopy gap, beam radiation can reach the gap floor via direct radiation (solid lines in Figure 2) and attenuated radiation (dotted lines in Figure 2). The gap can receive attenuated radiation only (Figure 3a) if the gap diameter is smaller than the maximum shadow length (D_{max}, Equation (4)) in the gap floor (Figure 2):

$$D_{max} = \frac{h}{\tan\alpha} \tag{4}$$

The light attenuation length (L_{xy}) for any given point *S(x,y)* in the gap floor (Figure 3) is given by

$$\begin{aligned} L_{xy} &= L_{max} - \frac{x}{\cos\alpha} \\ L_{max} &= \frac{h}{\sin\alpha} \end{aligned} \tag{5}$$

where L_{max} is the maximum attenuation length to the gap base.

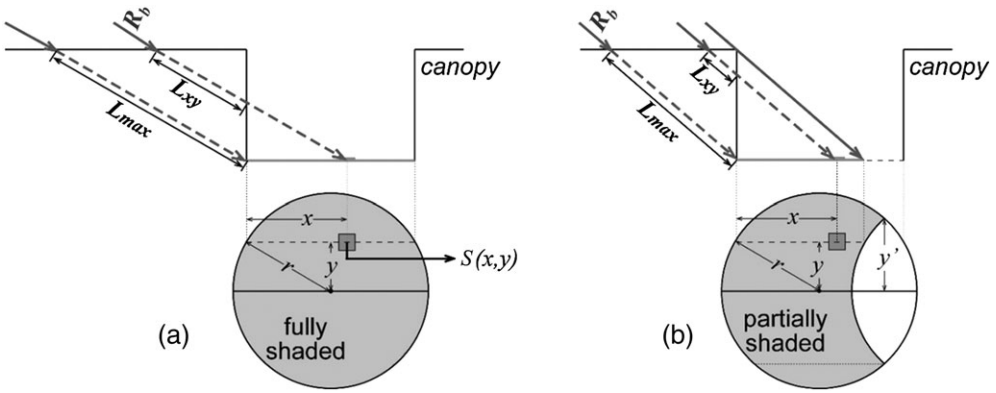

FIGURE 3 Cross-sectional view of shading geometry in a fully shaded (a) and a partially shaded (b) cylindrical gap, where *S(x,y)* is any given point in the gap base, *r* is the gap radius, R_b is downward beam radiation above the canopy, *L* is light attenuation length, and L_{max} is the maximum *L* at a given solar elevation angle

In the fully shaded condition (Figure 3a), or $D_{max} \geq 2r$, the total (attenuated) beam radiation incident on the gap floor ($\sum R_{b,g}$) is determined by summing the individual $R_{b,g}$ for every $S(x,y)$ over the gap base, leading to

$$\sum R_{b,g} = \frac{2R_b}{\pi r^2}\left(\int_0^r\int_0^{2\sqrt{r^2-y^2}} e^{-kL_{xy}}\,dxdy\right) \quad (6)$$

where R_b is the downward beam radiation above the canopy. In the partially shaded condition (Figure 3b), or $D_{max} < 2r$, the $\sum R_{b,g}$ is calculated as a sum of the attenuated radiation and direct radiation:

$$\sum R_{b,g} = \frac{2R_b}{\pi r^2}\left(\int_0^{y'}\int_0^{D_{max}} e^{-kL_{xy}}\,dxdy + \int_{y'}^r\int_0^{2\sqrt{r^2-y^2}} e^{-kL_{xy}}\,dxdy + \int_0^{y'}\int_{D_{max}}^{2\sqrt{r^2-y^2}}\,dxdy\right) \quad (7)$$

$$y' = \sqrt{r^2 - \frac{h^2}{4\tan^2\alpha}}$$

2.2.2 | Diffuse shortwave radiation

We estimated diffuse shortwave radiation in the canopy gap ($R_{d,g}$) using the original DHSVM formulation as in Equation (8) with the adjusted sky view factor (θ) given as a function of solar elevation and gap radius:

$$R_{d,g} = R_d[\theta + \tau_d(1-\theta)] \quad (8)$$

where R_d is the diffuse atmospheric radiation and τ_d is the canopy transmittance of diffuse radiation. We took the approach of Seyednasrollah and Kumar (2014) to estimate the sky view factor θ over the gap base:

$$SVF(y,x) = \frac{1}{\pi^2}\int_0^{2\pi}\tan^{-1}\left(\frac{\sqrt{R^2 - x^2\cdot\sin^2\alpha} - x\cdot\cos\alpha}{h}\right)d\alpha \quad (9)$$

$$\theta = \int_0^R SVF(y,x)dx$$

Diffuse shortwave radiation for the surrounding canopy ($R_{d,f}$) is calculated using the original DHSVM formulation:

$$R_{d,f} = R_d\tau_d \quad (10)$$

2.2.3 | Longwave radiation

The *NLW* on the gap snowpack was estimated using the original DHSVM formulation with an adjusted sky view factor (θ):

$$NLW = L_d\theta + (1-\theta)\cdot\sigma T_c^4 - \sigma T_s^4 \quad (11)$$

where L_d is the incoming longwave radiation from the atmosphere, σ is the Stephan–Boltzmann constant, T_c is the canopy temperature of the surrounding forest in Kelvin (which is commonly assumed to be the same as air temperature), and T_s is the surface temperature of gap snowpack in Kelvin. We did not account for the influence of terrain slope on θ, because *NLW* is rather insensitive to a changing slope from 0° to 30° (Seyednasrollah et al., 2013). Readers are referred to Wigmosta et al. (1994, 2002) for detailed descriptions and key formulations used in calculating undercanopy radiation fluxes.

2.3 | Wind velocity

The wind speed in the gap base is expected to fall between the speed under the continuous forest canopy and in an open area, due to the sheltering effect of the surrounding forest. Hence, we estimated the wind speed in the gap base as a weighted average of the wind speed under the continuous canopy and in the open. Without measurements, the weight parameter can be treated as a calibration parameter. Here, we set the weight equal to the areal fraction of the gap in the grid cell. Although we acknowledge that wind deposition and redistribution can be important for modelling snow accumulation and ablation processes, the DHSVM currently has no explicit representation of these processes.

3 | STUDY SITE AND DATA

The study area (Figure 4) is characterized by a transitional continental–maritime climate regime. We tested the model at three sites in Idaho, USA—an open reference site, a densely forested reference site, and a forest gap experimental site (Figure 4). The gap site is located in the Flat Creek unit of the University of Idaho Experimental Forest (UIEF) near Moscow, Idaho (46°51′16″N, 116°43′24″W). The gap is

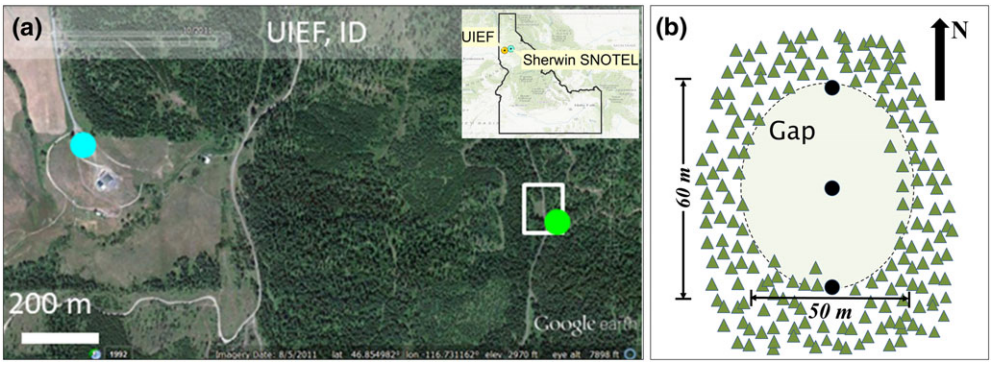

FIGURE 4 (a) Aerial view in 2011 showing the location of the open reference site (in blue dot), the forest reference site (in green dot), and the forest gap experimental site (in white box) in the University of Idaho experimental forest (UIEF; adapted from Dickerson-Lange et al., 2017). Location of the Sherwin SNOTEL relative to the UIEF is shown in the inset. (b) Schematic of the gap site adapted from Carson (2010). The black dots illustrate the snow sensors installed at the north, centre, and south edges of the N-S transect of the gap floor that provide snow measurements

approximately 60 m N-S by 50 m E-W surrounded by dense forest dominated by red cedar. The forest site is approximately 40 m to the southeast edge of the gap and is also dominated by red cedar. The sites are located on flat terrain that has negligible topographic impact on radiation. The open site is located at an exposed hilltop (46°51′17″N, 116°44′41″W) about 1.5 km west of the gap.

Continuous meteorological data and snow water equivalent (SWE) were measured at all three sites for the ablation period only (from mid-February through early May in 2008). At the gap site, meteorological data and SWE were measured along the N-S transect of the gap floor at the gap north edge, the gap centre, and the gap south edge. The data were collected every 5 s and were averaged and recorded every 30 min. The average air temperature collected in the open site showed a large range from −10.9 to 22.6 °C, indicating a colder than average winter. The observed 30 min wind speed in the open ranged from 0 to 8 m/s with an average value of 2.0 m/s compared with 0–2 m/s measured in the gap and forest. Bulk precipitation was measured locally using 5-gallon buckets and recorded at irregular intervals. The monitored radiation in the gap and SWE data in the open, forest, and gap sites were used for model validation. Readers are referred to Lawler and Link (2011), Carson (2010), and Dickerson-Lange et al. (2017) for more details on the experimental sites and setup, observational data collection, and the data processing procedure.

Recognizing the importance of snow accumulation for melt processes, we used the measurements of daily air temperature and precipitation from the nearby Sherwin SNOwpack TELemetry Network (SNOTEL) site (46°57′ N, 116°20′ W), approximately 30 km from the gap site, as the basis for creating meteorological input for the model for the snow accumulation period (when onsite meteorological measurements were unavailable). Note that the observed initial SWE is significantly different at the three sites. The open site accumulated the least snow and had an initial SWE of 113 mm, which was about 73% of the initial SWE in the forest (154 mm) and only about 35% of the SWE in the gap (327 mm). As noted by Dickerson-Lange et al. (2017), the UIEF sites are subject to high-wind storm events and the differential snow accumulation at the three sites is partially attributable to wind redistribution that was obvious at the open site. To account for the effects of wind drift, we scaled the SNOTEL precipitation data with a constant ratio (one for the open site and another for both the forest and gap sites) applied to the whole accumulation period so that the model simulated SWE matches the measured initial SWE at the three sites. The scaling factor was 0.51 for the open site and 0.73 for the gap and forest sites. Because wind speed data are not available from the SNOTEL, we used the wind speed field from the nearest surface meteorological point on a 1/16° grid produced by Livneh et al. (2013). Using the mountain microclimate simulation model (Hungerford, Nemani, Running, & Coughlan, 1989), daily air temperature and precipitation data from SNOTEL were disaggregated into smaller temporal steps assuming air temperature followed a sine curve and precipitation was constant over the day; incoming solar radiation was prescribed from solar geometry corrected for atmospheric transmittance (estimated from the maximum daily temperature range); and downward longwave radiation was estimated based on the Stefan–Boltzman equation adjusted for cloudiness (estimated from the maximum daily temperature range). All meteorological inputs during accumulation were disaggregated into the 30 min intervals to be consistent with the resolution of onsite meteorological measurements for the ablation period.

The DHSVM was configured to run a single 90 by 90 m model grid cell. The forest gap was characterized by a circular gap of 60 m diameter surrounded by 25 m tall canopy consistent with the actual forest stand height. The entire gap was treated as a single snowpack on the subgrid level of a model grid cell, on which a full mass and energy balance was employed in snow modelling. Meteorological input to the DHSVM consists of air temperature, precipitation, downward shortwave and longwave radiation, relative humidity, and wind velocity.

4 | RESULTS AND DISCUSSION

4.1 | Model evaluation

The model evaluation focused on the site observational data during the ablation period. The modelled (Equations (7), (8), and 11) gap-average (that assumes a uniform snowpack over the gap portion) subhourly *NSW* and incoming longwave radiation to the gap snowpack agreed well with the station measurements taken at the centre of the gap floor (Figure 5). The coefficient of determination (denoted by R^2) was 0.76 and 0.87 for *NSW* and incoming longwave radiation to the gap snowpack, respectively. Note that the observed and simulated values of incoming longwave radiation to the gap snowpack include the impacts of the surrounding forest.

At the open and forest sites, the SWEs of the station observations and the grid-average simulation (which assumes a uniform snowpack over the grid) were compared. The comparison showed a very high R^2 greater than 0.98 and a bias about 0.1 mm at both sites (Figure 6; Table 1). At the gap site, SWEs were compared between the simulated gap snowpack (separate from the forest snowpack) and the average SWE measured during the ablation period at three stations located at the north edge, centre, and south edge of the N-S transect of the circular gap floor. The comparison showed good agreement (Figure 6) with a R^2 of 0.94 and bias of 10.4 mm. The comparatively higher bias of modelled SWE in the gap was due mainly to the discernible deviation from observed SWE following small precipitation events (<1.5 mm/day) lasting for a few days at the end of March. The bias could be attributed to inaccurate precipitation records. Other likely contributing factors to the bias include the lack of a ground heat flux component in the model as the soil temperatures were noted to be relatively high (i.e., 0.5–1.0 °C) at the gap site (Carson, 2010), and the scale mismatch between point measurements and subgrid average simulations. Nonetheless, the model was able to reproduce the ablation pattern at all three sites with distinct vegetation cover, and is capable of representing the key processes that control the snow-cover dynamics under different vegetation covers on the grid spatial scale.

The comparison of simulated and observed snow disappearance date (or snow-free date with less than 0.5 mm SWE) showed a maximum error of 4 days at the gap site (Table 1). Both model simulations and observations showed that snow disappeared earliest in the open, about 40 days earlier than the fo

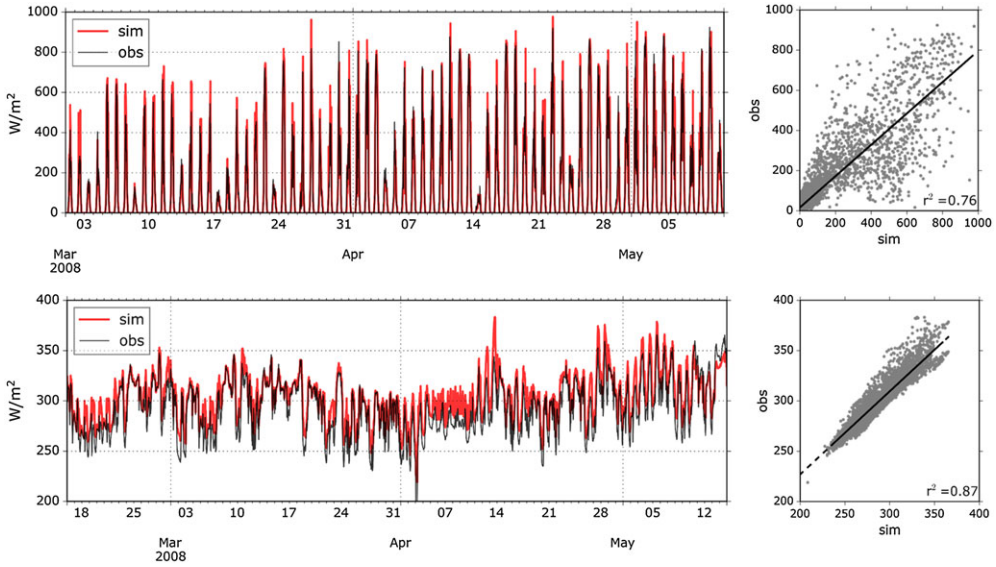

FIGURE 5 Comparison of measured and simulated subhourly net shortwave radiation (upper graphs) and incoming longwave radiation (lower graphs) at the centre of the gap floor. Note that the observed and simulated values used here include the impacts of surrounding forest on both shortwave and longwave radiation

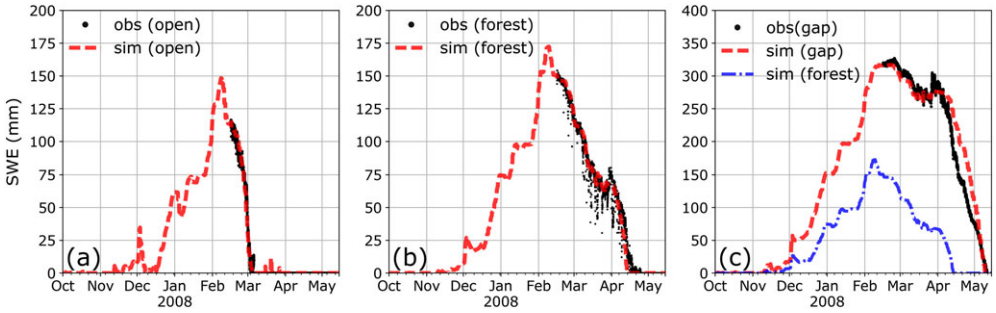

FIGURE 6 Comparison of the measured and modelled snow water equivalent (SWE) in the (a) open, (b) forest, and (c) gap sites. Note the different *y*-axis scales. In (c), the simulated SWE at the forest site is replotted on the same scale for comparison

TABLE 1 Summary metrics of simulated and observed mean ablation rate, SDD, and SWE bias during the ablation period

Site	SDD (mm/dd)		ΔSDD (days)	Ablation rate (mm/day)		R^2	SWE bias (mm)
	Obs	Sim		Obs	Sim		
Open	3/6	3/5	1	6.4	6.1	0.99	−0.1
Forest	4/20	4/16	4	2.6	2.5	0.98	−0.1
Gap	5/12	5/11	1	3.8	3.7	0.94	10.4

Note. ΔSDD = SDD(sim) − SDD(obs). Bias = (sim(SWE)-obs(SWE))/*n*, where *n* is the size of observations. SDD = snow disappearance day; SWE = snow water equivalent.

than in the gap. The modelled snow ablation pattern was generally in agreement with the measurements (Figure 7). The mean ablation rate over the melt season was highest in the open site, followed by the gap and then the forest sites. During the early phase of melting (i.e., early February–March), the melt rate was significantly higher in the open and the ablation rate in the forest was higher than in the gap. The reverse happened during the late melting phase (April–May), when the melt rate increased dramatically in the gap. Overall, the gap demonstrated marked temporal variability in ablation rates during the melt season (Figure 7).

4.2 | Snowpack energetics and ablation patterns

We analysed the modelled snowpack energy-balance terms to interpret the temporal variability of snowpack dynamics under different forest conditions. We calculated the monthly average values of the snowpack energy-balance components (as described in Equation (1)) from the subhourly model output (Figure 8). Heat input from rainfall was accounted for in the model but not included in the analyses, because the impact was negligible on the monthly scale, featuring limited occurrences and amounts of rainfall during the simulation period.

During the accumulation season (December to early February), the snowpack melt energy (ΔQ) was positive in the open and negative in the forest and gap. With low incoming shortwave radiation at low solar elevations, the *NLW* dominated the net radiation incident on snowpack at all three sites during accumulation. The *NLW* remained negative in the open and gap, and remained positive in the forest due to incoming longwave radiation emitted from the canopy. In the open, the primary sources contributing positively to ΔQ were *NSW* and *H*. The magnitude of turbulent fluxes (*H* + *LE*) in the open was much greater than in the forest and gap, where the average wind speed was lower due to the wind-sheltering effect of the canopy (note different *x*-axis scales in Figure 8). There is also a distinct effect of tc

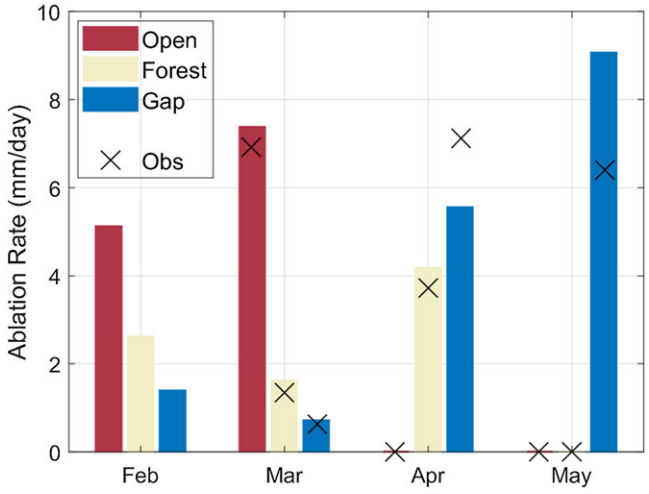

FIGURE 7 Simulated monthly ablation rates (unit: mm/day) in the open, forest, and gap sites when snow was present. Ablation rates calculated from snow water equivalent observations are marked by the symbol "X." The observed ablation rate is not calculated for February due to incomplete measurements

site because it is located in a valley bottom, even though the terrain is relatively low-relief. In the forest, the net radiation input was entirely compensated by the negative turbulent fluxes, which is likely caused by a higher snow surface temperature. At the gap site, the (negative) net radiation and (positive) turbulent fluxes largely cancelled each other resulting in a ΔQ close to zero.

During the early melt season (early February through March), the primary source for melt was net radiation dominated by *NSW* at all three sites. The total energy change was much higher in the open than in the forest and gap due to the lack of canopy attenuation of direct radiation, leading to a significantly higher ablation rate (Figure 8). The *NSW* in the gap was higher than in the forest due to the shorter attenuation path length through the canopy. However, the net radiation was higher in the forest (so was the ablation rate) due to enhanced longwave radiation from the canopy. This phenomenon was described by Lawler and Link (2011) as a type of radiative paradox in forest gaps: when solar elevations are relatively low in the early melt season, enhanced longwave radiation under canopy can offset reductions in shortwave radiation leading to higher net radiation relative to the gap floor. During the late melt season (April to mid-May), ΔQ was much higher in the gap than in the forest. The rapid increase of ΔQ in the gap was a result of greater *NSW* input, due to the reduced impact of light attenuation from the surrounding forest at higher solar elevations. In contrast, the snow-cover energetics in the forest showed little variation, due to the continuing dominant control of canopy attenuation on shortwave radiation and smaller temporal variability of *NLW*.

4.3 | Model structure evaluation

This section evaluates the extent to which the modified model relative to the original version makes the greatest difference in modelling gap snowpack dynamics. We ran the enhanced and original model using the same input and parameterization as described in Section 3, except that the gap radius *r* in the enhanced model varies from 2.5 to 45 m with a 2.5 m increment. Given the representative canopy height (h = 25 m) in the study sites, the size of gap was characterized by the ratio of gap radius to canopy height (r/h) and ranged from 0.1 to 1.8 as *r* varied between 2.5 and 45 m.

We compared the model-estimated SWE and snowpack ablation rates between the (circular) gap by the enhanced DHSVM and an areally equivalent open fraction (represented by 1-FC) by the original DHSVM (Figure 9). Because no interaction between the forested fraction (represented by FC in Figure 1) and the open fraction was accounted for on the grid level in the original model, simulated SWE and melt rate in the open or forested fraction by the original DHSVM did not change with changing r/h. Between the two versions of the model, we found greater difference in ablation rates in smaller gaps (i.e., smaller r/h). This was because, as r/h increased, the impact of the surrounding forest decreased on both *NSW* and *NLW* in the gap, leading to a more similar SWE pattern between the original and enhanced DHSVM. Further, the sensitivity of ablation rates simulated by the enhanced model changed with r/h. The snow ablation rate was most sensitive to changing r/h in medium-size gaps ($0.5 \leq r/h \leq 1.2$). In small gaps ($r/h < 0.5$) and large gaps ($r/h > 1.2$), there was little variability in ablation rate as r/h increased, although the ablation rate in large gaps was close to double that in the small gaps.

Compared with the original model that conceptualizes gaps as open areas independent from the surrounding forest, the estimated *NSW* in the gap from the enhanced model was consistently lower due to light attenuation of the surrounding forest, and the estimated

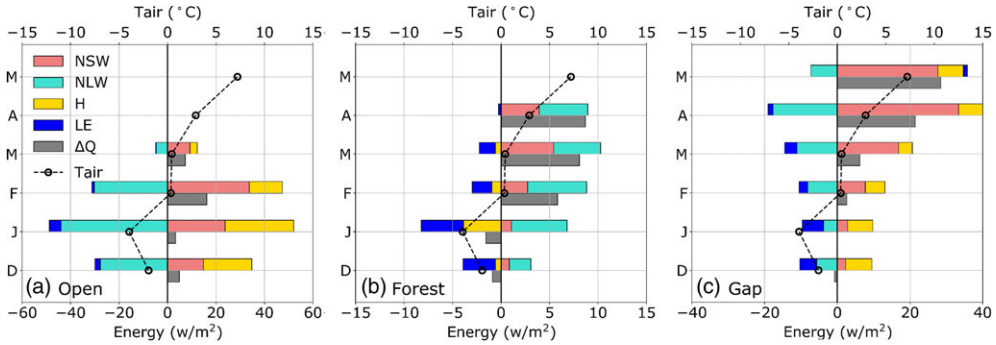

FIGURE 8 Simulated monthly snowpack energy balance components for the (a) open, (b) forest, and (c) gap sites when snow was present. *NSW* is net shortwave radiation, *NLW* is net longwave radiation, *H* is sensible heat flux, *LE* is latent heat flux, and ΔQ is available energy for snowmelt. Tair is mean monthly air temperature. If snow disappears in the beginning of a month, the energy fluxes for that month are not included in the plots. The heat input from rainfall is minimal and hence is not included in the plots. Note the different *x*-axi

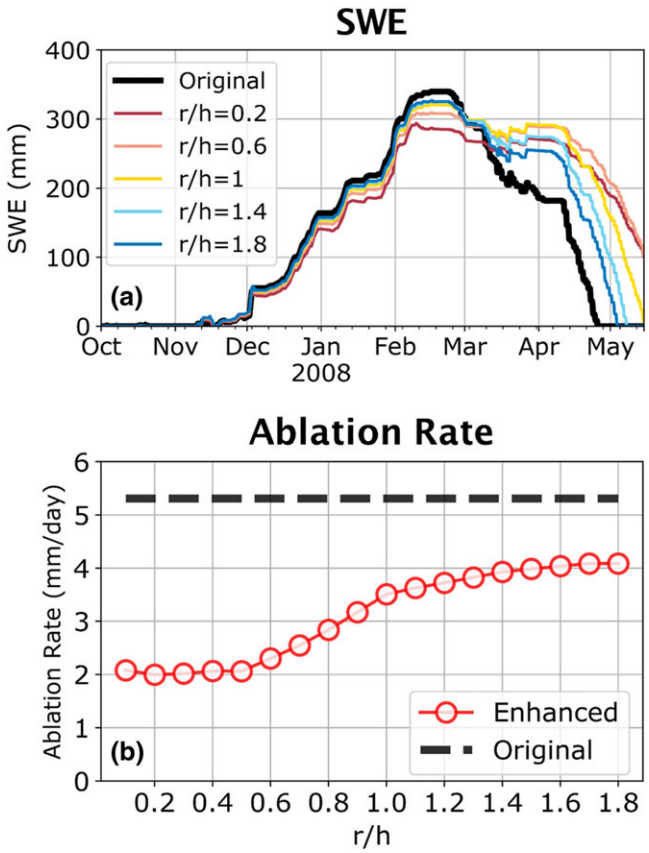

FIGURE 9 (a) Simulated snow water equivalent (SWE) for a range of gap sizes indicated by the ratio of gap radius to canopy height (*r/h*). SWE simulations end in mid-May when observed meteorological data are unavailable; (b) simulated ablation rates of gap snowpack for a range of *r/h* using the enhanced model, compared with simulated ablation rates in the open fraction in the original distributed hydrology soil vegetation model (represented by 1-FC in Figure 1). The label "Original" indicates the original distributed hydrology soil vegetation model that does not account for interaction between the forested fraction and open fraction in snow modelling

NLW was always higher than that in the original model due to the impact from the surrounding forest on the sky view factor (Figure 10). During the accumulation period, the variability of *NSW* with changing *r/h* was small because of limited incoming shortwave radiation at low solar elevations. The higher *NLW* estimated by the enhanced model explained the lower peak SWE, regardless of gap size, than the original model (Figure 9a). The turbulent fluxes increased with a greater *r/h*, and the variability with changing *r/h* was greater in small gaps (*r/h* < 0.5). In the original model, the higher *NSW* was essentially compensated by the negative *NLW*, leading to a negative and lower ΔQ compared with the enhanced model. During the melt season, the *NSW* increased rapidly with increasing *r/h*, especially during the late melt season with higher solar elevations (Figure 10b,c). In small and large gaps (*r/h* < 0.5 or *r/h* > 1.2), the increase in *NSW* was largely offset by the decrease in *NLW*, leading to relatively constant ablation rates. In medium-size gaps ($0.5 \leq r/h \leq 1.2$), with increasing *r/h*, the rate of increase in *NSW* became greater than the rate of decrease in *NLW*, resulting in greater sensitivity of ablation rates to *r/h*. There was an increasing trend of turbulent fluxes with a greater *r/h* that impacts wind speed. The magnitude of change was little compared with radiative fluxes during the melt season.

In practical implementation of canopy gaps that have the same total gap areas, a larger number of distributed small gaps can have greater potential for longer snow retention than a smaller number of large gaps. For example, a large gap of *r* = 30 m (i.e., *r/h* = 1.2) is equivalent to four gaps of *r* = 15 m (i.e., *r/h* = 0.6) in surface area, which is about 34.9% of the surface area in a 90 by 90 m grid cell. Assuming no interaction between the gaps, the grid-average SWE was calculated as the area-weighted SWE of the forest fraction and the gap(s). The smaller gaps were found to be able to retain snow for a longer period with a slightly reduced peak SWE compared with the larger gaps (Figure 11). For example, the grid cell with one large gap (*r* = 30 m) had a mean ablation rate of 3.0 mm/day, and the grid cell with four small gaps (*r* = 15 m) of equal gap area had a mean ablation rate of 2.5 mm/day. Grid-averaged peak SWE and snow duration were greater in all gap scenarios than in a forest-only (no gap) scenario.

4.4 | Watershed-scale streamflow implications

We selected the snow-dominated Chiwawa watershed on the eastern side of the Washington Cascade mountain range to demonstrate the impacts of forest gaps on streamflow and late-season low flows in particular (Figure 12). The watershed is about 446 km^2 in area and encompasses elevations ranging from 570 to 2,822 m. About 69% of the watershed is forest covered. Spring snowmelt is the primary source of river flows during the summer and early fall seasons characterized by low precipitation. As an important salmon spawning location in

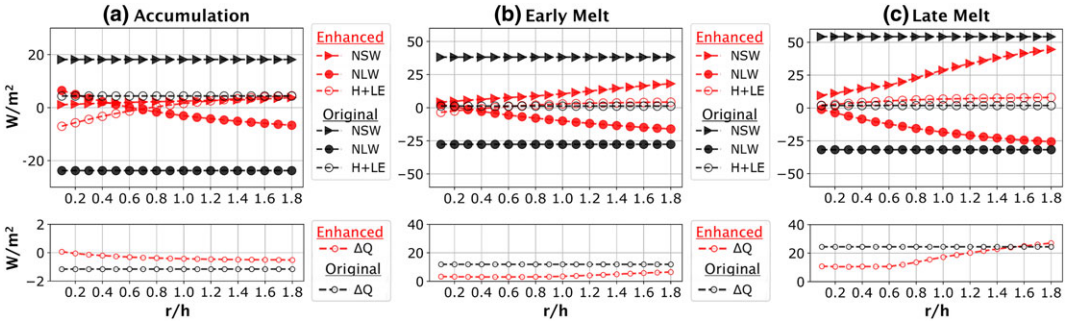

FIGURE 10 Comparison of modelled snowpack energy budget components (unit: W/m^2) during (a) the accumulation season, (b) the early melt season, and (c) the late melt season between the gap snowpack in the enhanced model and the areally equivalent open fraction in the original DHSVM for a range of *r/h* values. *NSW* is net shortwave radiation, *NLW* is net longwave radiation, *H + LE* is turbulent fluxes, ΔQ is available energy for snowmelt. Note the different *y*-axis scales

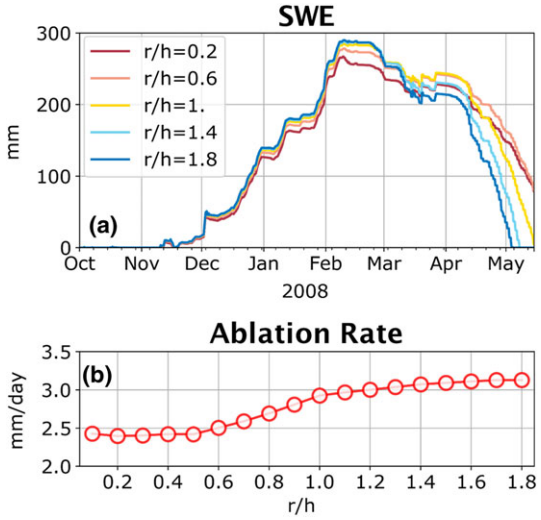

FIGURE 11 (a) Simulated grid-average snow water equivalent (SWE), and (b) simulated grid-average ablation rates for a 90 by 90 m grid cell with areally equivalent gap(s) with a range of gap sizes indicated by the ratio of gap radius to canopy height (r/h). The total gap area is about 35% of the total grid area. In this way, a large gap of r = 30 m (i.e., r/h = 1.2) is equivalent to four gaps of r = 15 m (i.e., r/h = 0.6) in surface area. SWE simulations end in mid-May when observed meteorological data are unavailable

Washington State, the late-season low flows in the Chiwawa River and associated increase in water temperature are of great concern because they can lead to reduction in habitat availability and water quality.

We ran the enhanced DHSVM at a 90 m scale and 3-hr time step for 30 years from Water Years (WY) 1974–2003, driven by the 1/16° gridded meteorological data of Livneh (Livneh et al., 2013). Other data used for model input and parameterization included the U.S. Geological Survey digital elevation model terrain data, the Natural Resources Conservation Service Soil Survey Geographic Database soil data, and the LANDFIRE vegetation data that provide information about the vegetation cover, canopy height, and overstory FC of forest covers (http://www.landfire.gov/index.php). The model-predicted daily SWE agreed plausibly well with SWE measurements collected at the Trinity SNOTEL station (48°4′ N, 120°51′ W) for WY 1993–2003 with a Nash-Sutcliffe Efficiency (NSE) of 0.8. The U.S. Geological Survey measured daily streamflows available from WY 1992–2003 at the basin outlet (gage 12456500) were used for model calibration and validation. The NSE of daily simulated flow was 0.86 for the calibration period of WY 1998–2003, and the NSE was 0.79 for the validation period of WY 1993–1998 (Figure 12). During the late-season low flow period (August through October) over WY 1998–2003, the daily low flow predictions had a R^2 of 0.6 and a percent bias of −6.5%, and the monthly low flow predictions had a R^2 of 1.0 and a percent bias of −6.0%.

With the calibrated DHSVM, we compared a simple gap scenario to a baseline consisting of the current vegetation without gaps. For the gap scenario, we created a 60 m gap for all (90 m) grid cells where forest canopy was 15–38 m in height and the FC was over 45% (based on the LANDFIRE data). As a result, the majority of the created gaps are medium-sized gaps ($0.8 \leq r/h \leq 1.2$), which have a greater potential for longer snow retention according to the results of the above analysis. The total area of the created gaps was about 24% of the total watershed drainage area (calculated by $\pi \cdot (30\text{m})^2/(90\text{m})^2 \cdot 69\%$). We compared annual and seasonal streamflows over 30-year historical runs between the baseline and gap scenarios (Figure 13). The results showed that the mean annual water yield with the gap scenario increased by 8.2% (or 7.5 cm/year) relative to the baseline scenario.

The gap scenario significantly increased the mean monthly flows (12.7–37.6% increase from the baseline) during the low flow period from late summer through fall (August through November). This could be attributed to greater snowpack depth, higher peak SWE, longer snowpack duration, and reduced evapotranspiration under the gap

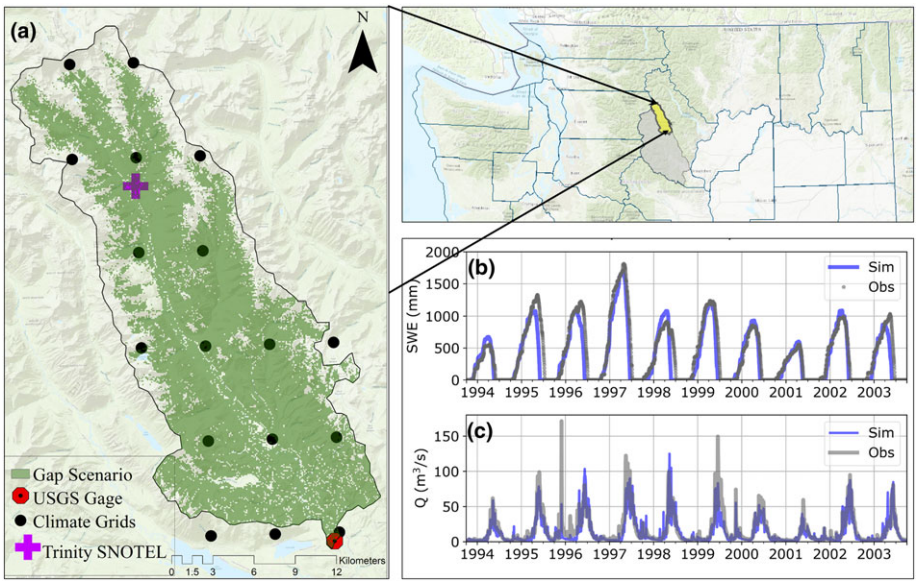

FIGURE 12 (a) The site map of the Chiwawa watershed on the eastern side of the Washington Cascade mountain range. The "Gap Scenario" indicates the forest cover (15–38 m in height with a fractional coverage over 45%) where canopy gaps are created; (b) the simulated versus observed daily snow water equivalent (SWE) at the Trinity SNOTEL station (48°4′ N, 120°51′ W); and (c) the simulated versus observed daily streamflow at U.S. Geological Survey (USGS) gage 12456500

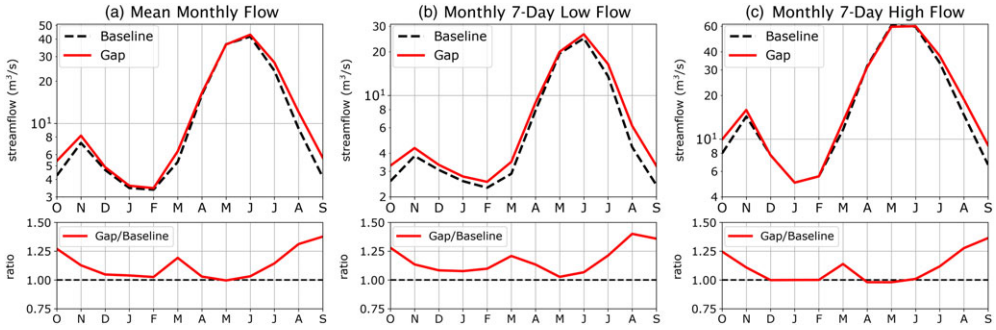

FIGURE 13 Comparison of (a) mean monthly flow, (b) mean monthly 7-day low flow, and (c) mean monthly 7-day high flow over the 30-year historical run between the baseline (current) vegetation and the gap scenarios. Note that the *y*-axis uses a log-10 scale. The lower panels shows the monthly flow ratio from the gap scenario to the baseline scenario

scenario. The impact of the gaps on streamflow weakens during the snow accumulation months (December through February) with a smaller increase from 2.5–4.7%. During the melt-driven high flow season (April to June), the gap scenario showed little change (0–3%) in mean monthly flows. Similar seasonal impacts were found in the mean monthly 7-day low flows and high flows. The gap scenario showed a much greater impact during late summer through fall. The greatest increase (40% or 1.76 m^3/s from the baseline) in the mean monthly 7-day low flows was observed in August, and the greatest increase (36.4% or 2.42 m^3/s) in the mean monthly 7-day high flows was observed in September. Under the gap scenario, the mean annual 7-day low flow was increased by 19.4% (or 0.37 m^3/s), whereas the impact on the mean annual 7-day high flows was negligible.

Here, we modelled a simplified gap implementation scenario and examined the seasonal streamflows at the Chiwawa basin outlet only. Further research is needed to more fully understand the effects of gap treatments on watershed hydrology under different physiographic conditions. As illustrated in Ellis et al. (2013), canopy gap treatments have the potential to de-synchronize snowmelt depending on watershed orientation (i.e., north- vs. south-facing slopes). With the enhanced model, we can further assess the impact of gap treatment on spring streamflow as a function of slope orientation. Similarly, the model applications of canopy gaps should be extended to different climate regimes. The snowmelt and streamflow responses are expected to vary with changing meteorological conditions (and associated radiation regimes), for example, maritime climate as opposed to continental climate. Lastly, from management perspectives, this enhanced model can be used to assess where (in the watershed) and what type of manipulation on canopy structure and/or characteristics will be most efficient for enhancing late-season streamflows across climate regimes.

5 | CONCLUSIONS

Here, we present the first research that explicitly assesses the effects of prescribed canopy gap treatments on watershed flow regimes that are linked to forest–snow interactions. We enhanced the distributed hydrological model DHSVM with an integral process-based canopy gap model that allows for detailed characterization of gap structure and snowpack evolution that is influenced by the surrounding forest. Through the model evaluations and applications, we conclude that

- The enhanced DHSVM is able to capture radiation and snowpack dynamics at a fine subhourly scale under distinct canopy covers (open, gap, and forest);
- At the UIEF experimental sites, canopy gaps significantly alter the magnitude and timing of spring snowmelt. Peak SWE in the gap was over two times more than that in the surrounding forest and open site, with snow duration over 1 and 2 months longer than in the forest and open, respectively. Notably, in contrast to the open and forest sites, snowmelt in the gap site exhibited significant temporal variability characterized by slower melt in late winter and early spring, followed by much more rapid melt in late spring due largely to the reduced radiation attenuation by the surrounding forest at high solar elevations.
- With the same total gap areas, a greater number of distributed small gaps can have greater potential for longer snow retention than a smaller number of large gaps.
- In the snow-dominated Chiwawa watershed, the prescribed canopy gap treatments demonstrate considerable potential for enhancing late-season low flows. With 24% of the watershed drainage area converted to gaps of 60 m diameter, the mean monthly 7-day low flows were increased by 13.5–40% during the low flow period from late summer through fall.

Future research is needed to more fully understand the effects of gap treatments on watershed flow regime under varying physiographic conditions (e.g., watershed slope orientation) and weather regimes. Potential model improvement could be made for more realistic representation of canopy structure (e.g., shape), as well as for snow interception and wind-related processes.

ACKNOWLEDGMENTS

This research by Pacific Northwest National Laboratory was supported jointly by a U.S. Department of Defense Strategic Environmental Research and Development Program grant (Project RC-2546) and the U.S. Department of Energy Bioenergy Technologies Office. The authors gratefully acknowledge Dr. Timothy Link and the University of Idaho for providing the observations used herein. The DHSVM source code is distributed through a git repository (https://github.com/pnnl/DHSVM-PNNL) that is made publicly available. The DHSVM tutorial and test data package will be published at htt

Timothy Link and an anonymous reviewer for their insightful comments and suggestions to improve this paper.

ORCID

Ning Sun http://orcid.org/0000-0002-4094-4482
Mark Wigmosta http://orcid.org/0000-0002-2918-8284
Tian Zhou http://orcid.org/0000-0003-1582-4005
Jessica Lundquist http://orcid.org/0000-0003-2193-5633
Susan Dickerson-Lange http://orcid.org/0000-0002-2157-4033
Nicoleta Cristea http://orcid.org/0000-0002-9091-0280

REFERENCES

Ambach, W. (1974). The influence of cloudiness on the net radiation balance of a snow surface with high albedo. *Journal of Glaciology*, *13*, 73–84. https://doi.org/10.1017/S0022143000023388

Anderson, H. W. (1963). Managing California's snow zone lands for water. Res. Paper PSW-RP-6. Berkeley, CA: Pacific Southwest Forest and Range Experiment Station, Forest Service, U S. Department of Agriculture; 28 p. 6, https://doi.org/10.1001/jama.1963.63710110006010a.

Barnett, T. P., Pierce, D. W., Hidalgo, H. G., Bonfils, C., Santer, B. D., Das, T., … Dettinger, M. D. (2008). Human-induced changes in the hydrology of the western United States. *Science*, *319*, 1080–1083. https://doi.org/10.1126/science.1152538

Beckers, J., Smerdon, B., & Wilson, M. (2009). Review of hydrologic models for forest management and climate change applications in British Columbia and Alberta. FORREX Series 25, Forum for Research and Extension in Natural Resources Society, Kamloops, British Columbia, Canada.

Berry, G., & Rothwell, R. (1992). Snow ablation in small forest openings in Southwest Alberta. *Canadian Journal of Forest Research*, *22*, 1326–1331. https://doi.org/10.1139/x92-176

Bowling, L. C., & Lettenmaier, D. P. (2001). The effects of forest roads and harvest on catchment hydrology in a mountainous maritime environment. In M. S. Wigmosta, & S. J. Burges (Eds.), *Land use and watersheds: Human influence on hydrology and geomorphology in urban and forest areas*. Washington, D. C: American Geophysical Union. https://doi.org/10.1029/WS002p0145

Broxton, P., Harpold, A., Biederman, J., Troch, P. A., Molotch, N., & Brooks, P. D. (2015). Quantifying the effects of vegetation structure on snow accumulation and ablation in mixed-conifer forests. *Ecohydrology*, *8*, 1073–1094. https://doi.org/10.1002/eco.1565

Cao, Q., Sun, N., Yearsley, J., Nijssen, B., & Lettenmaier, D. P. (2016). Climate and land cover effects on the temperature of Puget Sound streams. *Hydrological Processes*, *30*, 2286–2304. https://doi.org/10.1002/hyp.10784

Carson, R. D. (2010). Quantifications of snow pack mass and energy dynamics across a canopy discontinuity (unpublished Master's thesis). University of Idaho.

Church, J. E. (1912). The progress of Mount Rose Observatory, 1906–1912. *Science*, *36*, 796–800. https://doi.org/10.1126/science.36.936.796-a

Church, J. E. (1933). Snow surveying: Its principles and possibilities. *Geographical Review*, *23*, 529–563. https://doi.org/10.2307/209242

Connaughton, C. (1935). The accumulation and rate of melting of snow as influenced by vegetation. *Journal of Forestry*, *33*, 564–569.

Cristea, N. C., Lundquist, J. D., Loheide, S. P., Lowry, C. S., & Moore, C. E. (2014). Modelling how vegetation cover affects climate change impacts on streamflow timing and magnitude in the snowmelt-dominated upper Tuolumne Basin, Sierra Nevada. *Hydrological Processes*, *28*, 3896–3918. https://doi.org/10.1002/hyp.9909

Dickerson-Lange, S. E., Lutz, J. A., Martin, K. A., Raleigh, M. S., Gersonde, R., & Lundquist, J. D. (2015). Evaluating observational methods to quantify snow duration under diverse forest canopies. *Water Resources Research*, *51*, 1203–1224. https://doi.org/10.1002/2014WR015744

Dickerson-Lange, S. E., Gersonde, R. F., Hubbart, J. A., Link, T. E., Nolin, A. W., Perry, G. H., … Lundquist, J. D. (2017). Snow disappearance timing is dominated by forest effects on snow accumulation in warm winter climates of the Pacific Northwest, United States. *Hydrological Processes*, *31*(10), 1846–1862. https://doi.org/10.1002/hyp.11144

Du, E., Link, T. E., Gravelle, J. A., & Hubbart, J. A. (2014). Validation and sensitivity test of the distributed hydrology soil-vegetation model (DHSVM) in a forested mountain watershed. *Hydrological Processes*, *28*, 6196–6210. https://doi.org/10.1002/hyp.10110

Ellis, C., Pomeroy, J., & Link, T. (2013). Modeling increases in snowmelt yield and desynchronization resulting from forest gap-thinning treatments in a northern mountain headwater basin. *Water Resources Research*, *49*, 936–949. https://doi.org/10.1002/wrcr.20089

Fang, X., Pomeroy, J., Ellis, C., MacDonald, M., DeBeer, C., & Brown, T. (2013). Multi-variable evaluation of hydrological model predictions for a headwater basin in the Canadian Rocky Mountains. *Hydrology and Earth System Sciences*, *17*, 1635–1659. https://doi.org/10.5194/hess-17-1635-2013

Golding, D. L., & Swanson, R. H. (1986). Snow distribution patterns in clearings and adjacent forest. *Water Resources Research*, *22*, 1931–1940. https://doi.org/10.1029/WR022i013p01931

Hedstrom, N., & Pomeroy, J. (1998). Measurements and modelling of snow interception in the boreal forest. *Hydrological Processes*, *12*, 1611–1625. https://doi.org/10.1002/(SICI)1099-1085(199808/09)12:10/11%3C1611::AID-HYP684%3E3.0.CO;2-4

Hungerford, R. D., Nemani, R. R., Running, S. W., Coughlan, J. C. (1989). MTCLIM: A mountain microclimate simulation model. U.S. Forest Service Intermountain Research Station Research Paper INT-414, https://doi.org/10.1136/bjo.73.9.689.

Jost, G., Moore, R. D., Weiler, M., Gluns, D. R., & Alila, Y. (2009). Use of distributed snow measurements to test and improve a snowmelt model for predicting the effect of forest clear-cutting. *Journal of Hydrology*, *376*, 94–106. https://doi.org/10.1016/j.jhydrol.2009.07.017

Kern, C. C., Burton, J. I., Raymond, P., D'Amato, A. W., Keeton, W. S., Royo, A. A., … Willis, J. L. (2017). Challenges facing gap-based silviculture and possible solutions for mesic northern forests in North America. *Forestry*, *90*, 4–17. https://doi.org/10.1093/forestry/cpw024

Kittredge, J. (1953). Influences of forests on snow in the ponderosa, sugar pine, fir zone of the Central Sierra Nevada. *Hilgardia*, *22*, 1–96. https://doi.org/10.3733/hilg.v22n01p001

Lawler, R. R., & Link, T. E. (2011). Quantification of incoming all-wave radiation in discontinuous forest canopies with application to snowmelt prediction. *Hydrological Processes*, *25*, 3322–3331. https://doi.org/10.1002/hyp.8150

Leung, L. R., & Wigmosta, M. S. (1999). Potential climate change impacts on mountain watersheds in the Pacific Northwest. *JAWRA Journal of the American Water Resources Association*, *35*, 1463–1471. https://doi.org/10.1111/j.1752-1688.1999.tb04230.x

Lindner, M., Lasch, P., & Erhard, M. (2000). Alternative forest management strategies under climatic change-prospects for gap model applications in risk analyses. *Silva Fennica*, *34*, 101–111.

Link, T. E., & Marks, D. (1999). Point simulation of seasonal snow cover dynamics beneath boreal forest canopies. *Journal of Geophysical Research*, *104*, 27841–27857.

Livneh, B., Deems, J. S., Buma, B., Barsugli, J. J., Schneider, D., Molotch, N. P., … Wessman, C. A. (2015). Catchment response to bark beetle outbreak and dust-on-snow in the Colorado Rocky Mountains. *Journal of Hydrology*, *523*, 196–210. https://doi.org/10.1016/j.jhydrol.2015.01.039

Livneh, B., Rosenberg, E. A., Lin, C., Nijssen, B., Mishra, V., Andreadis, K. M., … Lettenmaier, D. P. (2013). A long-term hydrologically based dataset of land surface fluxes and states for the conterminous United States: Update and extensions*. *Journal of Climate*, *26*, 9384–9392. https://doi.org/10.1175/JCLI-D-12-005

Lundquist, J. D., Dickerson-Lange, S. E., Lutz, J. A., & Cristea, N. C. (2013). Lower forest density enhances snow retention in regions with warmer winters: A global framework developed from plot-scale observations and modeling. *Water Resources Research*, *49*, 6356–6370. https://doi.org/10.1002/wrcr.20504

Marks, D., Kimball, J., Tingey, D., & Link, T. (1998). The sensitivity of snowmelt processes to climate conditions and forest cover during rain-on-snow: A case study of the 1996 Pacific Northwest flood. *Hydrological Processes*, *12*, 1569–1587. https://doi.org/10.1002/(SICI)1099-1085(199808/09)12:10/11%3C1569::AID-HYP682%3E3.0.CO;2-L

McCabe, G. J., & Clark, M. P. (2005). Trends and variability in snowmelt runoff in the western United States. *Journal of Hydrometeorology*, *6*, 476–482. https://doi.org/10.1175/JHM428.1

McCabe, G. J., Hay, L. E., & Clark, M. P. (2007). Rain-on-snow events in the western United States. *Bulletin of the American Meteorological Society*, *88*, 319–328. https://doi.org/10.1175/BAMS-88-3-319

Moeser, D., Morsdorf, F., & Jonas, T. (2015). Novel forest structure metrics from airborne LiDAR data for improved snow interception estimation. *Agricultural and Forest Meteorology*, *208*, 40–49. https://doi.org/10.1016/j.agrformet.2015.04.013

Moeser, D., Stähli, M., & Jonas, T. (2015). Improved snow interception modeling using canopy parameters derived from airborne LIDAR data. *Water Resources Research*, *51*, 5041–5059. https://doi.org/10.1002/2014WR016724

Moore, C. A., & McCaughey, W. W. (1997). Snow accumulation under various forest stand densities at Tenderfoot Creek Experimental Forest, Montana, USA. https://doi.org/10.1080/09595239800187491.

Murray, C., & Buttle, J. (2003). Impacts of clearcut harvesting on snow accumulation and melt in a northern hardwood forest. *Journal of Hydrology*, *271*, 197–212. https://doi.org/10.1016/S0022-1694(02)000352-9

Musselman, K. N., Molotch, N. P., Margulis, S. A., Lehning, M., & Gustafsson, D. (2012). Improved snowmelt simulations with a canopy model forced with photo-derived direct beam canopy transmissivity. *Water Resources Research*, *48*, W10509. https://doi.org/10.1029/2012WR012285

Nowak, D. J., Hoehn, R. E., Bodine, A. R., Greenfield, E. J., Ellis, A., Endreny, T. A., … Henry, R. (2013). Assessing urban forest effects and values: Toronto's urban forest. Resour. Bull. NRS-79. Newtown Square, PA: U.S. Department of Agriculture, Forest Service, Northern Research Station. 59 p.

Peixoto, J. P., & Oort, A. H. (1992). *Physics of climate*. (p. 520). New York: American Institute of Physics.

Pomeroy, J., Gray, D., Brown, T., Hedstrom, N., Quinton, W., Granger, R., & Carey, S. (2007). The cold regions hydrological model: A platform for basing process representation and model structure on physical evidence. *Hydrological Processes*, *21*, 2650–2667. https://doi.org/10.1002/hyp.6787

Pomeroy, J., Gray, D., Shook, K., Toth, B., Essery, R., Pietroniro, A., & Hedstrom, N. (1998). An evaluation of snow accumulation and ablation processes for land surface modelling. *Hydrological Processes*, *12*, 2339–2367. https://doi.org/10.1002/(SICI)1099-1085(199812)12:15%3C2339::AID-HYP800%3E3.0.CO;2-L

Pomeroy, J., Marks, D., Link, T., Ellis, C., Hardy, J., Rowlands, A., & Granger, R. (2009). The impact of coniferous forest temperature on incoming longwave radiation to melting snow. *Hydrological Processes*, *23*, 2513–2525. https://doi.org/10.1002/hyp.7325

Pomeroy, J., Parviainen, J., Hedstrom, N., & Gray, D. (1998). Coupled modelling of forest snow interception and sublimation. *Hydrological Processes*, *12*, 2317–2337. https://doi.org/10.1002/(SICI)1099-1085(199812)12:15%3C2317::AID-HYP799%3E3.0.CO;2-X

Regonda, S. K., Rajagopalan, B., Clark, M., & Pitlick, J. (2005). Seasonal cycle shifts in hydroclimatology over the western United States. *Journal of Climate*, *18*, 372–384. https://doi.org/10.1175/JCLI-3272.1

Reifsnyder, W. E., & Lull, H. W. (1965). Radiant energy in relation to forests. Technical Bulletin No. 1344. U. S. Dept. of Agriculture, Forest Service.

Seyednasrollah, B., & Kumar, M. (2014). Net radiation in a snow-covered discontinuous forest gap for a range of gap sizes and topographic configurations. *Journal of Geophysical Research: Atmospheres*, *119*, 10,323–10,342. https://doi.org/10.1002/2014JD021809

Seyednasrollah, B., Kumar, M., & Link, T. E. (2013). On the role of vegetation density on net snow cover radiation at the forest floor. *Journal of Geophysical Research: Atmospheres*, *118*, 8359–8374.

Sicart, J. E., Essery, R. L., Pomeroy, J. W., Hardy, J., Link, T., & Marks, D. (2004). A sensitivity study of daytime net radiation during snowmelt to forest canopy and atmospheric conditions. *Journal of Hydrometeorology*, *5*, 774–784. https://doi.org/10.1175/1525-7541(2004)005%3C0774:ASSODN%3E2.0.CO;2

Stednick, J. D. (1996). Monitoring the effects of timber harvest on annual water yield. *Journal of Hydrology*, *176*, 79–95. https://doi.org/10.1016/0022-1694(95)02780-7

Stewart, I. T., Cayan, D. R., & Dettinger, M. D. (2005). Changes toward earlier streamflow timing across western North America. *Journal of Climate*, *18*, 1136–1155. https://doi.org/10.1175/JCLI3321.1

Storck, P., Bowling, L., Wetherbee, P., & Lettenmaier, D. (1998). Application of a GIS-based distributed hydrology model for prediction of forest harvest effects on peak stream flow in the Pacific northwest. *Hydrological Processes*, *12*, 889–904. https://doi.org/10.1002/(SICI)1099-1085(199805)12:6%3C889::AID-HYP661%3E3.0.CO;2-P

Sun, N., Yearsley, J., Voisin, N., & Lettenmaier, D. P. (2015). A spatially distributed model for the assessment of land use impacts on stream temperature in small urban watersheds. *Hydrological Processes*, *29*(10), 2331–2345. https://doi.org/10.1002/hyp.10363

Thyer, M., Beckers, J., Spittlehouse, D., Alila, Y., & Winkler, R. (2004). Diagnosing a distributed hydrologic model for two high-elevation forested catchments based on detailed stand-and basin-scale data. *Water Resources Research*, *40*, W01103. https://doi.org/10.1029/2003WR002414

Troendle, C. A., & King, R. M. (1985). The effect of timber harvest on the Fool Creek watershed, 30 years later. *Water Resources Research*, *21*, 1915–1922. https://doi.org/10.1029/WR021i012p01915

Varhola, A., Coops, N. C., Weiler, M., & Moore, R. D. (2010). Forest canopy effects on snow accumulation and ablation: An integrative review of empirical results. *Journal of Hydrology*, *392*, 219–233. https://doi.org/10.1016/j.jhydrol.2010.08.009

Whitaker, A., Alila, Y., Beckers, J., & Toews, D. (2002). Evaluating peak flow sensitivity to clear-cutting in different elevation bands of a snowmelt-dominated mountainous catchment. *Water Resources Research*, *38*, 1172–1188. https://doi.org/10.1029/2001WR000514

Wigmosta, M. S., Nijssen, B., Storck, P., & Lettenmaier, D. (2002). The distributed hydrology soil vegetation model. In V. P. Singh (Ed.), *Mathematical models of small watershed hydrology and applications* (pp. 7–42). Highlands Ranch, Colo: Water Resour. Publ.

Wigmosta, M. S., Vail, L. W., & Lettenmaier, D. P. (1994). A distributed hydrology-vegetation model for complex terrain. *Water Resources Research*, *30*, 1665–1679. https://doi.org/10.1029/94WR00436

Yan, H., Sun, N., Wigmosta, M., Skaggs, R., Hou, Z., & Leung, R. (2018). Next-generation intensity-duration-frequency curves for hydrologic design in snow-dominated environments. *Water Resources Research*, *54*(2), 1093–1108. https://doi.org/10.1002/2017WR021290

How to cite this article: Sun N, Wigmosta M, Zhou T, Lundquist J, Dickerson-Lange S, Cristea N. Evaluating the functionality and streamflow impacts of explicitly modelling forest–snow interactions and canopy gaps in a distributed hydrologic model. *Hydrological Processes*. 2018;1–13. https://doi.org/10.1002/hyp.13150